Journal of Power Sources 258 (2014) 117–121

Contents lists available at ScienceDirect

Journal of Power Sources

journal homepage: www.elsevier.com/locate/jpowsour

Short communication

PtRu nanofiber alloy counter electrodes for dye-sensitized solar cells

Hongyuan Cai [a], Qunwei Tang [a,*], Benlin He [a], Pinjiang Li [b]

[a] Institute of Materials Science and Engineering, Ocean University of China, Qingdao 266100, China
[b] Institute of Surface Micro and Nano Materials, Xuchang University, Xuchang 461000, China

HIGHLIGHTS

- Novel PtRu nanofiber alloys are prepared by a low-temperature hydrothermal method.
- The counter electrodes from PtRu alloys have superior electrocatalytic activity.
- A promising power conversion efficiency of 6.80% is recorded from $PtRu_3$ alloy CE.
- The new concept is instructive in designing DSSCs.

GRAPHICAL ABSTRACT

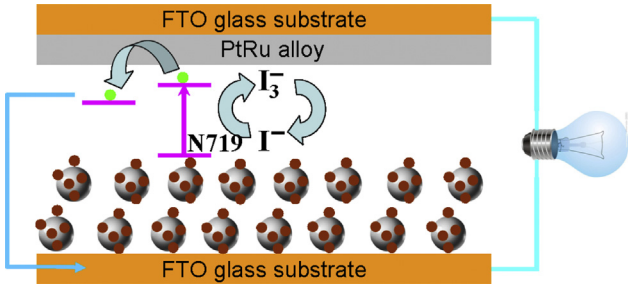

ARTICLE INFO

Article history:
Received 3 December 2013
Received in revised form
16 January 2014
Accepted 6 February 2014
Available online 15 February 2014

Keywords:
Dye-sensitized solar cell
PtRu alloy
Counter electrode
Nanofiber

ABSTRACT

With an aim of enhancing the light-to-electric power conversion efficiency of dye-sensitized solar cell (DSSC), here we synthesize PtRu nanofiber alloys using a low-temperature hydrothermal technique which are employed as counter electrodes (CEs) for DSSCs. Owing to the good electrical conduction and electrocatalysis, light-to-electric power conversion efficiencies of PtRu-based DSSCs have been elevated in comparison with that of Pt CE based DSSC. The DSSC employing $PtRu_3$ alloy CE gives a power conversion efficiency of 6.80% in comparison with 6.17% from Pt-based DSSC. The reasonable conversion efficiency, simple preparation, and scalability demonstrate the potential use of PtRu alloys in efficient DSSCs.

1. Introduction

Nowadays, low-carbon economy is a developing direction in human society. However, the excess consumption of fossil energy (coal, oil, and gas) has brought severe risks in energy depletion, environmental pollution, and ecological destruction. As an alternative energy source, solar energy has attracted growing interests because it is clean, inexhaustible, and geographically independent [1,2]. Among various solar cells, dye-sensitized solar cells (DSSCs) [3–8], electrochemical devices converting solar energy into electricity directly with no pollution emission, are honored by relatively low fabrication cost, high power conversion efficiency, and environmental friendliness. As a crucial component, Pt counter electrode (CE) plays a role in regenerating I^-/I_3^- redox species, which is originated from the electrocatalytic activity of Pt CE [9,10].

With an aim of elevating the electrocatalytic behaviors of CE toward triiodides and therefore photovoltaic performances of assembled DSSC devices, new CEs should be developed before their commercial applications. Here we report the design of PtRu nanofiber alloy CE by a low-temperature hydrothermal method. Alloy CEs are fresh in DSSC devices but they have displayed impressive functions in improving photovoltaic performances. Recently, $Co_{0.85}Se$ and $Ni_{0.85}Se$ alloy CEs from Wang et al. exhibited much higher electrocatalytic activity than Pt for redox reaction of

* Corresponding author. Tel./fax: +86 532 66781690.
E-mail address: tangqunwei@hotmail.com (Q. Tang).

http://dx.doi.org/10.1016/j.jpowsour.2014.02.022
0378-7753/

iodide/triiodide (I^-/I_3^-) couples [11]. The assembled DSSC from $Co_{0.85}Se$ CE generated a promising power conversion efficiency of 9.40%. Moreover, Au–Ag binary alloy can also be employed as counter electrode material in DSSC, demonstrating a conversion efficiency of 7.85% [12]. In the current work, the proposed PtRu nanofiber alloy CEs are also expected to have good electrocatalytic activity toward triiodides, on the basis of which the photovoltaic performances of DSSCs can be improved.

2. Experimental

2.1. Preparation of PtRu nanofiber alloy CEs

The feasibility of this strategy was confirmed by following experimental procedures: A mixing aqueous solution consisting of H_2PtCl_6 and $RuCl_3$ was made by agitating 5 ml of 20 mM H_2PtCl_6 and 20 mM $RuCl_3$ aqueous solutions. The volumes of the $RuCl_3$ aqueous solution were controlled at 0, 5, 15, and 20 ml. The total volume of the reactant solution was adjusted to 35 ml by deionized water. The reactant was transferred into a Teflon-lined autoclave and cleaned FTO glass substrate (sheet resistance 12 Ω square^{-1}, purchased from Hartford Glass Co., USA) with FTO layer downward was immersed in. After the reaction at 120 °C for 12 h, the FTO substrate was rinsed by deionized water and vacuum dried at 50 °C.

2.2. Assembly of DSSCs

A layer of TiO_2 colloid film with a thickness of 10 μm and area of 0.25 cm^2 was prepared by a sol-hydrothermal method and subsequently calcined at 450 °C for 30 min. The resultant TiO_2 nanocrystalline film was sensitized by immersing into a 0.50 mM ethanol solution of N719 dye (purchased from DYESOL LTD) for 24 h. A DSSC device was fabricated by sandwiching redox electrolyte between a dye-sensitized TiO_2 anode and an FTO supported PtRu nanofiber alloy CE. A redox electrolyte consisted of 100 mM of tetraethylammonium iodide, 100 mM of tetramethylammonium iodide, 100 mM of tetrabutylammonium iodide, 100 mM of NaI, 100 mM of KI, 100 mM of LiI, 50 mM of I_2, and 500 mM of 4-tert-butyl-pyridine in 50 ml acetonitrile.

2.3. Electrochemical characterizations

The electrochemical performances were recorded on a conventional CHI660E setup comprising an Ag/AgCl reference electrode, a CE of platinum sheet, and a working electrode of FTO glass supported PtRu alloy. The cyclic voltammetry (CV) curves were recorded in a supporting electrolyte consisting of 50 mM LiI, 10 mM I_2, and 500 mM $LiClO_4$ in acetonitrile. Electrochemical impedance spectroscopy (EIS) measurements were carried out in a frequency range of 0.01 Hz ~ 10^6 kHz and at an ac amplitude of 10 mV. Tafel polarization curves were recorded by assembling symmetric cell consisting of FTO/PtRu alloy|redox electrolyte|FTO/PtRu alloy.

2.4. Photovoltaic measurements

The photocurrent–voltage (J–V) curves of the DSSCs were recorded on an electrochemical workstation (CHI600E) under irradiation of a simulated solar light from a 100 W xenon arc lamp in ambient atmosphere. The incident light intensity was calibrated using an FZ-A type radiometer from Beijing Normal University Photoelectric Instrument Factory to control it at 100 mW cm^{-2} (AM 1.5). Each DSSC device was measured five times to eliminate experimental error and a compromise J–V curve was employed.

2.5. Other characterizations

The morphologies of the Ru and PtRu nanofiber alloy CEs were observed with a scanning electron microscope (SEM, S4800). The X-ray diffraction (XRD) data were collected in the 2θ range between 30 and 80° at a scanning speed of 10° min^{-1}. The compositions of

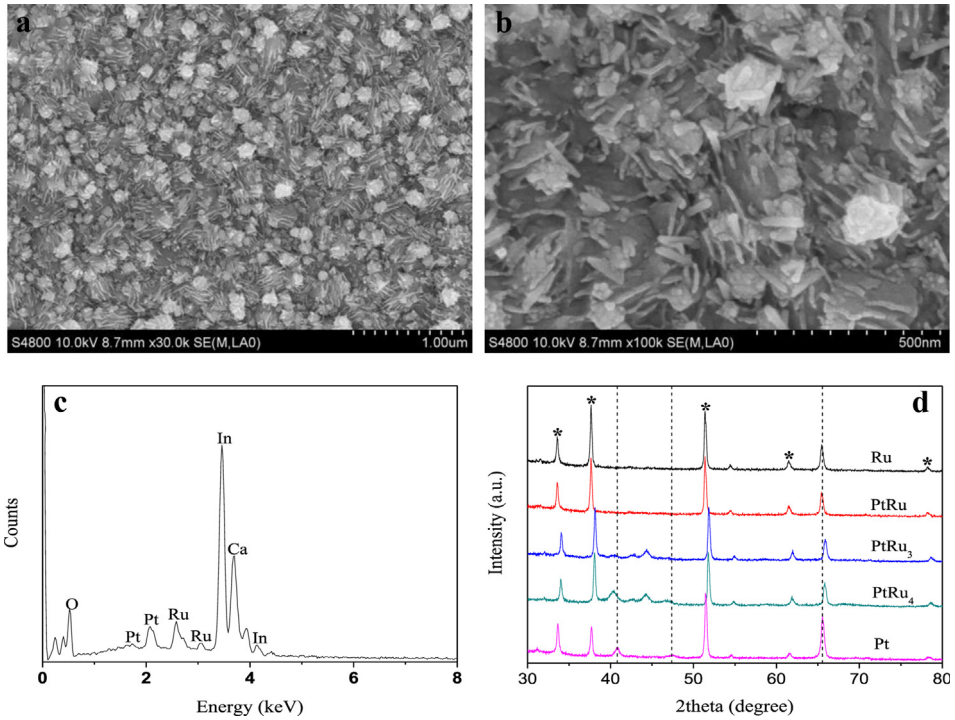

Fig. 1. (a) & (b) Top-view SEM images and (c) energy-dispersive X-ray spectrum of $PtRu_3$ nanofiber alloy CE; (d) XRD patterns of varied PtRu nanofiber alloy CEs. The peaks marked by (*) are from FTO glass substrate.

the alloy CEs were detected by inductively coupled plasma-atomic emission spectra (ICP-AES). Prior to ICP measurements, the alloy CEs were immersed in concentration nitric acid to dissolve the FTO glass substrate thoroughly.

3. Results and discussion

Top-view SEM photograph in Fig. 1a suggests a high surface coverage of $PtRu_3$ alloy on FTO substrate. Deep examination in Fig. 1b gives homogeneously nanofibers with a length of ~80 nm and a diameter of ~10 nm. From energy-dispersive X-ray (EDX) spectrum, as shown in Fig. 1c, Pt and Ru elements as well as the elements from FTO substrate are detected, indicating that Pt and Ru have been successfully codeposited on FTO glass substrate. The recorded contents of Pt and Ru from EDX spectrum are 1.22 and 3.49 mol%, respectively, giving an approximate ratio of 1:3. Moreover, the compositions of the alloys on FTO glass substrate were determined by ICP-AES equipment. The results display that the atomic ratios of PtRu, $PtRu_3$, and $PtRu_4$ are 1.00:0.95, 1.00:2.87, and 1.00:3.92, respectively. The measured atomic ratios are close to the stoichiometry of PtRu, $PtRu_3$, and $PtRu_4$, therefore, the chemical formulas of the alloy CEs can be expressed according to their stoichiometric ratios. The XRD patterns in Fig. 1d indicate that the presence of diffraction peaks at 40.8°, 47.4°, and 65.5°, which can be assigned to Pt(111), Pt(200), and Pt(220), consistent with the face-centered cubic (fcc) structure of Pt [13]. The PtRu alloys display diffraction patterns similar to those of Pt, except 2θ values are shifted to higher values. This indicates that single-phase PtRu alloy is formed [14,15]. Assuming alloy formation between Pt and Ru based on a substitutional solid solution, such as shift is attributed to the difference in atomic size between Pt and Ru atoms [16] or the formation of a high degree of PtRu alloy [17]. No diffraction peaks for tetragonal RuO_2 or hexagonally close packed Ru phases are detected, revealing that PtRu nanofiber catalyst is the main phase formed at atomic level with a basically unaltered Pt fcc structure [18]. The synergistic effect of Pt and Ru is expected to elevate the electrocatalytic activity of PtRu alloy toward triiodides.

The top-view SEM photographs of pure Ru, PtRu, and $PtRu_4$ alloy CEs are shown in Fig. 2 to determine the surface morphology evolution. A dense agglomerate is detected in Fig. 2a, suggesting that there are no nanofibers in pure Ru CE. Interestingly, we can find indications on the formation of nanofibers in PtRu alloy CE, as is shown in Fig. 2b. With increase of Ru dosage in alloy CE, such as $PtRu_4$ in Fig. 2c, the dimension of the nanofibers is increased in comparison with $PtRu_3$ alloys.

In the CV curves, as shown in Fig. 3a, the peak shapes of pure Ru and nanofiber alloy CEs are very similar to that of Pt electrode [19], showing that nanofiber alloy CEs have electrocatalytic function to I_3^-/I^- redox species. Differently, the peak positions of pure Ru and PtRu alloy CEs are more negative in comparison with pure Pt electrode. It is believed that the electrocatalytic activity of a CE dependent on two factors: peak position and peak current density. A more negative peak position indicates that the occurrence of electrocatalytic reaction is more difficult, however, a higher peak current density means that the reaction kinetics is more active. Although the peak position of $PtRu_3$ nanofiber alloy CE is more

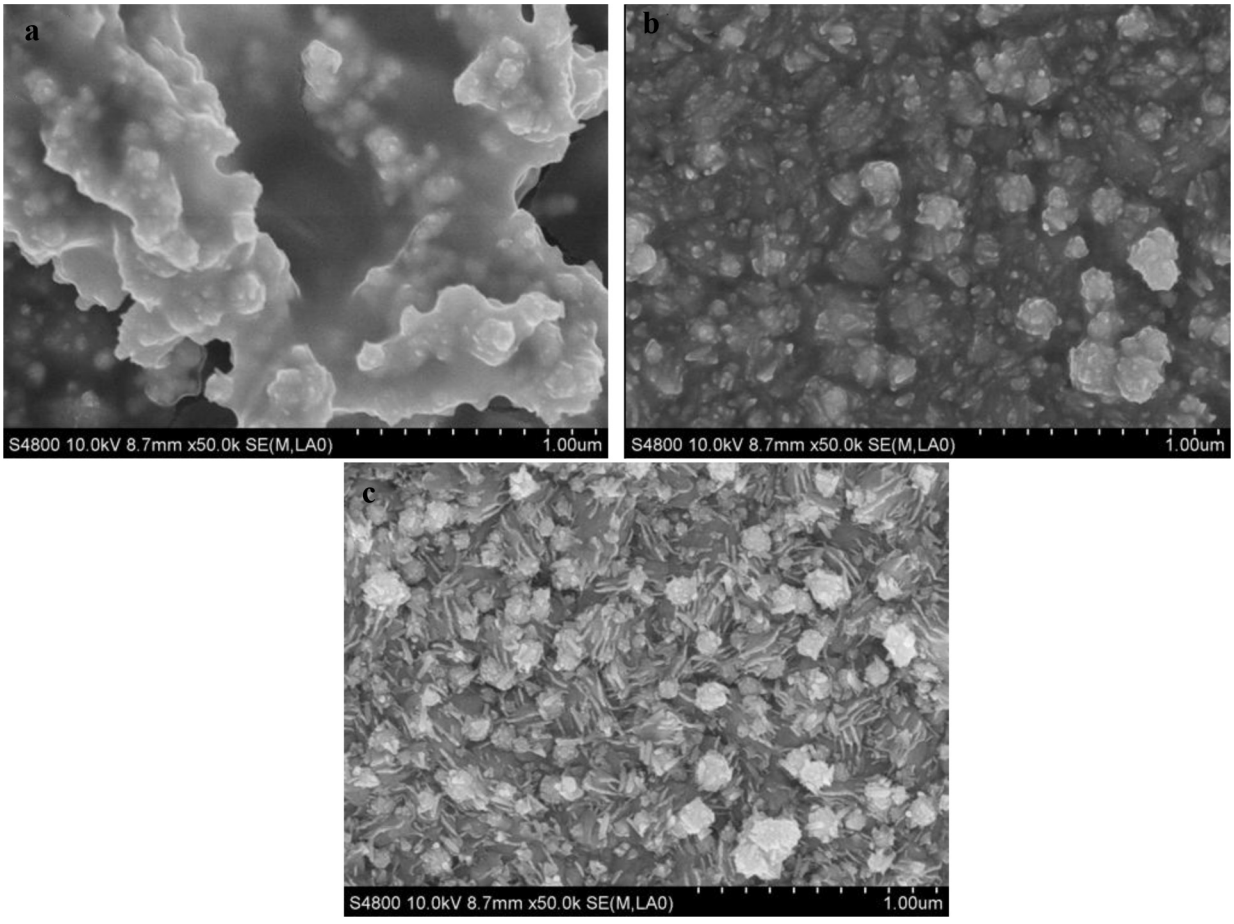

Fig. 2. Top-view SEM images of (a) Ru, (b) PtRu, and (c) $PtRu_4$ CEs.

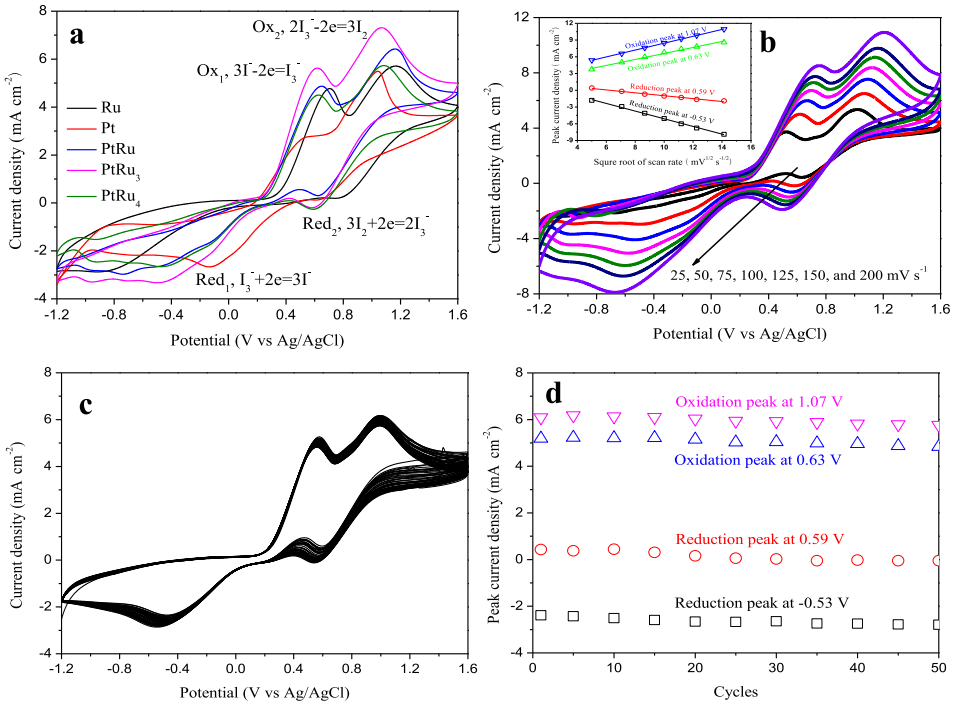

Fig. 3. (a) CV curves of various CEs recorded at a scan rate of 50 mV s^{-1}; (b) CV curves of $PtRu_3$ nanofiber alloy CE at various scan rates. The inset is relationship between peak current density and square root of scan rate; (c) 50 cycles of CV curves from $PtRu_3$ nanofiber alloy CE at various scan rates. The scan rate is 50 mV s^{-1}; (d) relationship between peak current density and cycle number.

negative than that of benchmark Pt CE (300–400 μm in thickness, purchased from Dalian HepatChroma SolarTech Co., Ltd), a peak current density enhancement of 1.3-fold is achieved for $PtRu_3$ nanofiber alloy CE. The better performance of the $PtRu_3$ nanofiber alloy CE is explained by a synergistic effect for reduction of triiodides ions, which is popular in electrocatalysts of fuel cells [20].

From the stacking CV curves of $PtRu_3$ nanofiber alloy CE at different scan rates, one can find an outward extension of all the

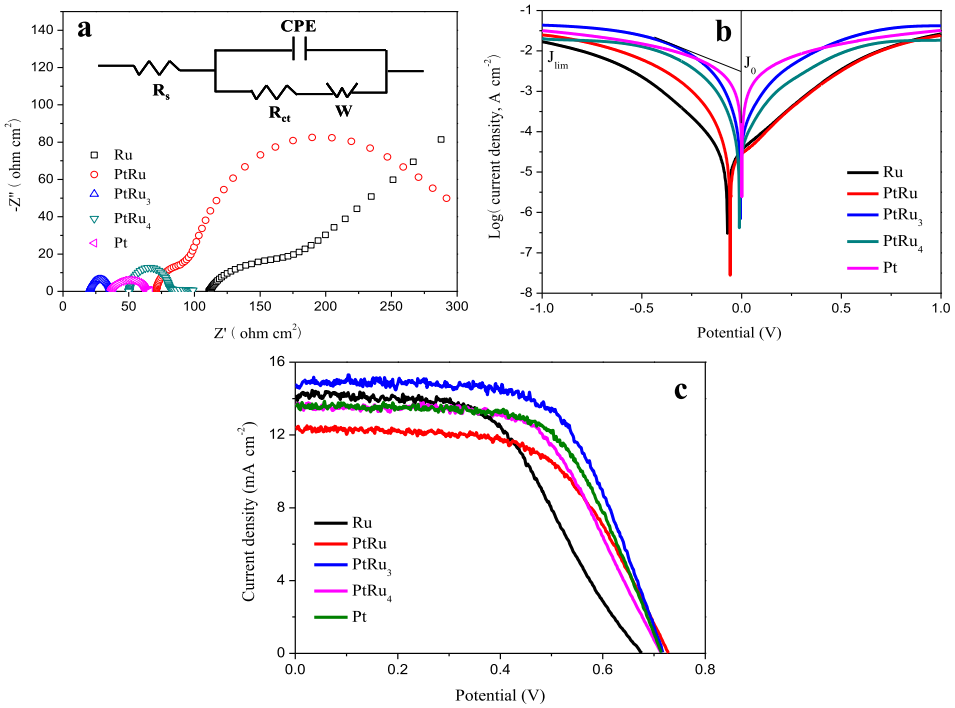

Fig. 4. (a) EIS spectra and (b) Tafel polarization curves of symmetrical cells fabricated various CEs; (c) characteristic *J–V* curves of DSSCs from varied CEs. The inset gives the equivalent circuit.

Table 1
The parameters derived from EIS plots, Tafel curves, and DSSC devices.

CEs	EIS parameters			Tafel parameters		Photovoltaic parameters			
	R_s (Ω cm^2)	R_{ct} (Ω cm^2)	W (Ω cm^2)	J_0 (mA cm^{-2})	J_{lim} (mA cm^{-2})	V_{oc} (mV)	J_{sc} (mA cm^{-2})	FF (%)	η (%)
Pt	37.1	25.5	5.32	2.16	33.57	713.9	13.55	63.8	6.17
Ru	111.5	51.8	7.57	0.014	16.56	675.2	14.03	52.9	5.01
PtRu	70.7	21.0	6.18	0.13	25.00	728.5	12.39	58.5	5.28
$PtRu_3$	20.7	14.1	4.25	0.31	42.56	718.3	14.70	64.4	6.80
$PtRu_4$	50.1	32.6	5.67	0.67	20.99	712.6	13.67	60.1	5.85

peaks (Fig. 3b). By plotting peak current density corresponding to $I_3^- \leftrightarrow I^-$ versus square root of scan rate, as shown in insert of Fig. 3b, linear relationships are observed. This result indicates the redox reaction is a diffusion-controlled mechanism on PtRu alloy CEs [21]. 50 cycles of CV curves in Fig. 3c are used to evaluate stability of $PtRu_3$ alloy CE and the plots of peak current density as a function of cycle number are given in Fig. 3d. No apparent decline in peak current densities is observed, indicating that the PtRu nanofiber alloy CEs are stable for catalyzing triiodides.

Nyquist plots in Fig. 4a illustrate impedance characteristics of various CEs. According to the Randles-type circuit (insert of Fig. 4a), the intercept on the real axis represents the series resistance (R_s), a reflection of CE resistance. The first arc arises from the charge-transfer resistance (R_{ct}) at CE/electrolyte interface, whereas W represents the Nernst diffusion impedance corresponding to the diffusion resistance of I^-/I_3^- redox species. CPE is a constant phase element and is frequently used as a substitute for a capacitor in an equivalent circuit to fit the impedance behavior of the electrical double layer. Except for $PtRu_3$, the R_{ct} values of PtRu alloys and pure Ru are all larger than that of Pt electrode, indicating an enhanced charge-transfer ability in $PtRu_3$ nanofiber alloy CE. W is of highly dependence on the electrical conduction of a CE [22]. The electrical conduction of the CE material can be evaluated by R_s value, therefore, the W value follows an order of $PtRu_3 < Pt < PtRu_4 < PtRu < Ru$. The conclusions for the electrocatalytic activity and charge-transfer derived from EIS and CV data are in a good agreement. Tafel polarization curves are presented in Fig. 4b by recording on the symmetrical cells to reveal the interfacial charge-transfer properties at the CE/electrolyte interface. The larger slope for the anodic or cathodic branch indicates a higher exchange current density (J_0) on the electrode and better catalytic activity toward triiodide reduction. Apparently, the calculated J_0 also follows an order of $PtRu_3 > Pt > PtRu_4 > PtRu > Ru$, which matches the order of R_{ct}. The elevated J_0 is the result of rapid charge-transfer [21]. The intersection of the cathodic branch with the Y-axis can be considered as the limiting diffusion current density (J_{lim}), which can be employed to assess diffusion properties of the redox couples. One can see that the J_{lim} also follows an order of $PtRu_3 > Pt > PtRu_4 > PtRu > Ru$.

Fig. 4c shows the photovoltaic characteristics of DSSCs from pure Pt, pure Ru, and various PtRu nanofiber alloy CEs. Table 1 summarizes the photovoltaic parameters using various CEs. The DSSCs employing $PtRu_3$ nanofiber alloy CE achieves the highest J_{sc} and power conversion efficiency (η). This might be attributed to a fact that $PtRu_3$ nanofiber alloy CE has a homogeneous nanofiber structure, which provides larger active surface areas for I_3^- reduction. The specific surface area of all the alloy CEs are measured by Brunauer–Emmett–Teller (BET) method, giving BET values of 72.6, 201.8, and 135.2 m^2 g^{-1} for PtRu, $PtRu_3$, and $PtRu_4$, respectively. A recorded η from $PtRu_3$-based DSSC is 6.80% in comparison with 6.17% in the DSSC of pure Pt CE and 5.01% in the DSSC from Ru CE.

4. Conclusions

In summary, we have demonstrated that low-temperature hydrothermal synthesis of PtRu alloy CEs is an effective strategy for enhancing the photovoltaic performances of DSSCs. $PtRu_3$ nanofiber alloy CE exhibits good electrocatalytic activity for the reduction of triiodide ions. The DSSC from $PtRu_3$ alloy CE provides an impressive power conversion efficiency of 6.80% in comparison with that of 6.17% from pure Pt CE. The research presented here is far from being optimized but these profound advantages along with scalable materials promise the new alloy CEs to be candidates in DSSCs.

Acknowledgments

The authors gratefully acknowledge Ocean University of China for providing Seed Fund to this project, and Fundamental Research Funds for the Central Universities (201313001, 201312005), Shandong Province Outstanding Youth Scientist Foundation Plan (BS2013CL015), Doctoral Fund of Ministry of Education of China (20130132120023), Shandong Provincial Natural Science Foundation (ZR2011BQ017), and Research Project for the Application Foundation in Qingdao (13-1-4-198-jch).

References

[1] A.J. Nozik, J. Miller, Chem. Rev. 110 (2010) 6443.
[2] A. Dewan, S.U. Ay, M.N. Karim, H. Beyenal, J. Power Sources 245 (2014) 129.
[3] B. O'Regan, M. Grätzel, Nature 353 (1991) 737.
[4] M. Grätzel, Nature 414 (2001) 338.
[5] Z. Huo, C.N. Zhang, X.Q. Fang, M. Cai, S.Y. Dai, K. Wang, J. Power Sources 195 (2010) 4384.
[6] S.S. Yuan, Q.W. Tang, B.L. He, P.Z. Yang, J. Power Sources 254 (2014) 98.
[7] Q.W. Tang, H.Y. Cai, S.S. Yuan, X. Wang, J. Mater. Chem. A 1 (2013) 317.
[8] Q.H. Li, X.X. Chen, Q.W. Tang, H.Y. Cai, Y.C. Qin, B.L. He, et al., J. Power Sources 248 (2014) 923.
[9] Y. Wang, C. Zhao, M. Wu, W. Lu, T.L. Ma, Electrochim. Acta 105 (2013) 671.
[10] V.D. Dao, S.H. Kim, H.S. Choi, J.H. Kim, H.O. Park, J.K. Lee, J. Phys. Chem. C 115 (2011) 25529.
[11] F. Gong, H. Wang, X. Xu, G. Zhou, Z.S. Wang, J. Am. Chem. Soc. 134 (2012) 10953.
[12] Q. Xu, F. Liu, Y. Liu, K. Cui, X. Feng, W. Zhang, Y. Huang, Sci. Rep. 3 (2013) 2112.
[13] S. Wang, X. Wang, S.P. Jiang, Langmuir 24 (2008) 10505.
[14] Z. Liu, J.Y. Lee, W. Chen, M. Han, L.M. Gan, Langmuir 20 (2004) 181.
[15] H. Li, G. Sun, Y. Gao, Q. Jiang, Z. Jia, Q. Xin, J. Phys. Chem. C 111 (2007) 15192.
[16] K.W. Park, J.H. Choi, K.S. Ahn, Y.E. Sung, J. Phys. Chem. B 108 (2004) 5989.
[17] A.K. Shukla, A.S. Arico, K.M. El-Khatib, H. Kim, P.L. Antonucci, V. Antonucci, Appl. Surf. Sci. 137 (1999) 20.
[18] R. Basnayake, Z. Li, S. Katar, W. Zhou, H. Rivera, E.S. Smotkin, et al., Langmuir 22 (2006) 10446.
[19] Z.Y. Tang, J.H. Wu, M. Zheng, J.H. Huo, Z. Lan, Nano Energy 2 (2013) 622.
[20] H.N. Dinh, X. Ren, F.H. Garzon, P. Zelenay, S. Gottesfeld, J. Electroanal. Chem. 491 (2000) 222.
[21] W. Zeng, G.J. Fang, X.Q. Wang, Q. Zheng, B.R. Li, H.H. Huang, et al., J. Power Sources 229 (2013) 102.
[22] J. Chen, B. Li, J. Zheng, J. Zhao, H. Jing, Z. Zhu, Electrochim. Acta 56 (2011) 4624.